The Role of Microexplosions in Flame Spray Synthesis for Homogeneous Nanopowders from Low-Cost Metal Precursors

Christopher D. Rosebrock, Thomas Wriedt, and Lutz Mädler
Foundation Institute of Material Science (IWT), Dept. of Production Engineering, University of Bremen, Badgasteiner Straße 3, 28359 Bremen, Germany

Karsten Wegner
Particle Technology Laboratory, Dept. of Mechanical and Process Engineering, ETH Zürich, Sonneggstrasse 3, 8092 Zürich, Switzerland

DOI 10.1002/aic.15056
Published online October 1, 2015 in Wiley Online Library (wileyonlinelibrary.com)

One of the most versatile and rapid manufacturing processes for a variety of nanopowders is flame spray pyrolysis (FSP). The production costs of this scalable process are largely controlled by the raw materials, pushing for the utilization of low-cost metal precursors. These, however, typically yield inhomogeneous products containing large particles up to micrometer size along with fine nanoparticles. Here, the release mechanism of nitrate and carboxylate precursors from spray droplets has been investigated by single-droplet combustion experiments and thermogravimetric analysis. The results show that neither precursor evaporation nor choice of solvents is prerequisite for homogeneous nanopowders but droplet microexplosions with continuing combustion. It is shown that even low-cost metal nitrates yield homogeneous nanopowders if precursors are formulated such that droplet microexplosions occur by internal superheating. The proposed precursor release mechanisms are verified with lab- and pilot-scale FSP, demonstrating that single-droplet combustion experiments can be employed to predict the product quality. © 2015 American Institute of Chemical Engineers *AIChE J*, 62: 381–391, 2016
Keywords: droplet combustion, gas-to-particle conversion, droplet-to-particle conversion, microexplosions, flame extinction

Introduction

Nanoparticles are attractive for a large variety of industrial applications, for instance, reinforcement agents, pigments, electronics, catalysts, or sensors.[1–4] Different routes are available for their manufacture such as solution precipitation or flame synthesis.[5,6] In particular, flame spray pyrolysis (FSP)[7] is able to readily produce highly pure, single- and multicomponent nanoparticles based on almost all elements in one process step.[8] A broad range of liquid and solid compounds such as metal organics (e.g., alkoxides, acetylacetonates, metal-carbocylic acid complexes) or inorganic metal salts (e.g. nitrates) can be utilized as precursors by diluting or dissolving them in predominantly organic solvents prior to combustion in a spray flame. The precursors are estimated the largest cost factor in industrial nanopowder production by FSP,[9] urging for the use of low-cost raw materials.

However, the choice and formulation of the liquid precursor/solvent feed drastically affects product nanopowder characteristics through droplet atomization, vaporization, and precursor release.[10,11] These processes depend on the physicochemical properties of the liquid feed, mainly viscosity, surface tension, volatility, thermal, and chemical stability as well as combustion enthalpy of the components. They can either lead to homogeneous nanopowders by gas-to-particle conversion or products with bimodal size distribution and micron-sized particle "contaminations" formed through the droplet-to-particle route.[4,12,13] Highly volatile but usually expensive precursors such as metal alkoxides typically produce homogeneous powders of agglomerated fine primary nanoparticles with monomodal size distribution. Inexpensive metal acetates, nitrates, or carbonates on the other hand frequently yield mixtures of nanoparticles and much larger dense or hollow spheres.

Mädler et al.[14] produced ceria nanoparticles from cerium acetate/acetic acid solutions and reported large particles of several hundred nanometers formed by droplet-to-particle conversion in addition to fine dense agglomerated nanoparticles by gas-to-particle conversion. By adding iso-octane to the precursor solution, homogeneous nanopowders were obtained. They concluded that the higher combustion enthalpy content of the iso-octane solution enhanced precursor vaporization and promoted gas-to-particle conversion. Jossen et al.[12] postulated that large combustion enthalpies (>4.7 kJ/g_{gas}) and ratios of the solvent boiling point to the precursor melting point (T_{bp}/T_{mp}) greater than unity lead to homogeneous nanopowders, while large and partially hollow particles are observed for lower combustion enthalpies and temperature ratios. Later, Jossen et al.[15] observed that their former combustion enthalpy criteria need to be increased to low boiling/melting point temperature ratios, since

Correspondence concerning this article should be addressed to L. Mädler at lmaedler@iwt.uni-bremen.de.

inhomogeneous nanopowders of yttrium-stabilized zirconia were obtained although the combustion enthalpy density was twice their recommended value. The authors concluded that the crystal water of the yttrium nitrate precursor may have reacted with the water-sensitive zirconium propoxide, forming intermediates with high melting/boiling point and leading to droplet shell formation. Mädler et al.[16] obtained homogeneous fine dense and agglomerated Bi_2O_3 nanopowders for bismuth nitrate precursor solutions by exchanging the solvent from ethanol to acetic acid, suggesting that droplet vaporization is promoted by the formation of more volatile intermediates such as acetobismuth complexes. Stark et al.[17] observed that homogeneous $Ce_{0.5}Zr_{0.5}O_2$ nanoparticles could be prepared employing carboxylic acid as solvent for cerium(III) acetate hydrate and zirconium(IV) acetylacetonate. They assumed that decarboxylation is taking place during vaporization, triggering droplet explosion from CO_2 release. Recently, Strobel and Pratsinis[13] showed that homogeneous nanoparticles from metal nitrates can be produced with addition of carboxylic acid, attributed to carboxylate formation that facilitates droplet vaporization and subsequent gas-to-particle conversion. These assumptions are in accordance with Rosebrock et al.,[10] who observed microexplosions for carboxylate precursor droplets.

Although it has been recognized that droplet-to-particle conversion is taking place for precursors with low volatility and leads to inhomogeneous product powders, the mechanisms of solvent and precursor release from droplets in high-temperature environment are far from being understood. Here, these mechanisms are studied for metal nitrates and carboxylates with the help of single-droplet combustion experiments and thermogravimetric analysis (TGA). The effect of precursor as well as different solvents on the combustion behavior is elaborated first for zinc oxide and then for iron and aluminum oxides. Based on this, conditions are developed that lead to homogeneous product nanopowders also for inexpensive nitrate precursors. The proposed mechanisms are verified by nanoparticle synthesis with lab- and pilot-scale FSP.

Experimental

The set-up for the single burning droplet experiments that has been described in detail by Rosebrock et al.[10] is shown schematically in Figure 1. It consists of the droplet-on-demand generator (piezodropper)[18,19] and a square cuvette. Single monodisperse droplets are ejected upward in coflowing 0.4 L/min oxygen (purity 99.95%) and ignited by a synchronized spark discharge. The droplet diameter is monitored with a high-speed camera (IDT—Motion Pro Y4L) at a frequency of 32,000 Hz by using a MATLAB-based edge detection program.[10] The different precursor/solvent mixtures are fed to the piezodropper from a small reservoir containing the precursor solutions.

Precursor solutions employed for ZnO nanoparticle synthesis were zinc nitrate hexahydrate (Sigma Aldrich, >99% purity) dissolved in ethanol (VWR, 99.8% purity) and zinc naphthenate (Alfa Aesar, 67 wt % naphthenate in white spirits) diluted with ethanol or xylene (VWR, 98.5% purity) to Zn concentrations of 0.1, 0.25, or 0.5 mol/L. Further, iron nitrate nonahydrate (Sigma Aldrich, >98% purity) and aluminum nitrate nonahydrate (Sigma Aldrich, >98% purity) were dissolved to 0.5 mol/L either in ethanol or a 1:1:1:1 by volume mixture of ethanol, xylene, diethyleneglycol monobutylether (Sigma Aldrich, 98% purity), and 2-ethylhexanoic acid (Sigma Aldrich, 99% purity) as described by Strobel and Pratsinis.[13]

Lab-scale production of nanopowders was performed with an FSP reactor described in detail by Mädler et al.[7] In brevity,

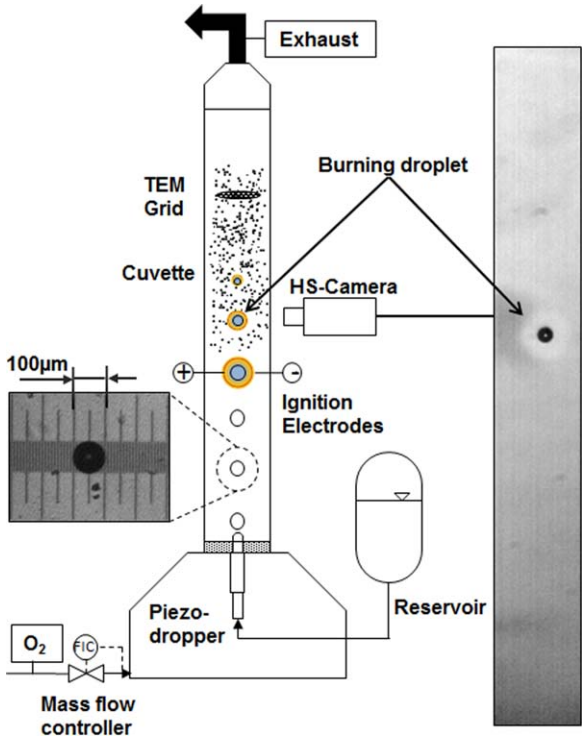

Figure 1. Single burning droplet set-up with piezodropper, precursor solution feed reservoir, mass flow controller for oxygen supply, cuvette, ignition electrodes, high speed camera, and TEM-grid holder.

[Color figure can be viewed in the online issue, which is available at wileyonlinelibrary.com.]

the metal precursor/solvent solutions were fed at 5 mL/min to the twin-fluid atomizer with a syringe pump and atomized with 5 L/min of oxygen at 1.5 bar pressure drop across the dispersion gas gap. The ignition of the resulting spray was accomplished with six flamelets of premixed 1.5 L/min CH_4 and 3.2 L/min O_2.

Furthermore, ZnO nanoparticle formation was studied in a pilot-scale FSP reactor described by Gröhn et al.[20]. The precursor was supplied to the twin-fluid atomizer of the FSP reactor with a syringe pump at 64 mL/min and atomized with 80 L/min of oxygen at 3 bar pressure drop across the dispersion gas gap. The resulting spray was ignited with a pilot flame of 2 L/min CH_4 and 4.5 L/min O_2 supplied through concentric annular channels.

Remnants of droplets and/or nanoparticles produced in single droplet combustion were collected on carbon-coated copper grids (Plano GmbH—S162) placed 5 cm above the ignition electrodes into the flow (Figure 1). Nanoparticles made with the lab- and pilot-scale reactors were sampled thermophoretically[21] on these grids at 5, 15, and/or 25 cm height above the burner (HAB). Nanoparticle size and morphology was characterized by transmission electron microscopy (TEM) (FEI Titan 80-300 or Tecnai F30, both operating with an acceleration voltage of 300 kV).

Thermogravimetric analysis (Netzsch STA 449 Jupiter) was conducted to assess the vaporization behavior of the different precursor solutions. Weight losses and signals from differential scanning calorimetry (DSC) were recorded while heating ~30 mg of the 0.5 mol/L precursor solutions placed in 70 μL

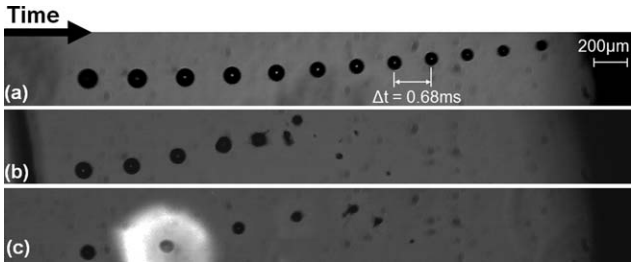

Figure 2. Image sequences of single burning droplets composed of 0.5 mol/L (a) Zn-nitrate/ethanol, (b) Zn-naphthenate/ethanol, and (c) Zn-naphthenate/xylene.

The time interval between two successive droplet images is 0.68 ms. The initial droplet diameters are (a) 134 μm, (b) 109 μm, and (c) 96 μm.

platinum crucibles in 50 mL/min synthetic air from 30 to 600°C at 7.5°C/min.

Results and Discussion

Zinc oxide

Image sequences of burning single droplets of (a) Zn-nitrate/ethanol (~7.5 ms), (b) Zn-naphthenate/ethanol (~5.1 ms), and (c) Zn-naphthenate/xylene (~4.1 ms) are shown in Figure 2. First, the nitrate-based droplet (a) continuously decreases in size by vaporization and combustion of the vapor in a flame surrounding the droplet.[10] The vaporization rate then ceases at the end of the image sequence, indicating flame extinction. In contrast, both Zn-naphthenate droplets (b and c) undergo microexplosions after a short period of stable burning (1.7 and 1.5 ms).

The shattered droplet fragments each continue to burn and again explode cascade-like, until the droplet fragments are completely consumed. This different combustion behavior of nitrate- and naphthenate-based precursor droplets might be the reason for the typically observed formation of homogeneous nanopowders from naphthenate or 2-ethylhexanoate precursors contrary to the inhomogeneous nanoparticles from nitrates.[12,13,16,17]

Figure 3 shows the evolution of the averaged normalized squared droplet diameter for 0.5 (green), 0.25 (red), and 0.1 (blue) mol/L Zn-nitrate/ethanol solutions as well as pure ethanol (black) based on the quantitative analysis of at least 10 different image sequences as seen in Figure 2a. Since the single-droplet experiments are highly reproducible,[10] the standard deviation between the different image sequences is less than the resolution limit of the high-speed camera (<3.5 μm per pixel) and has therefore been omitted. Droplet shrinkage proceeds similarly for all nitrate solutions until the squared droplet diameter has decreased to ~40% of the initial value d_0^2. Vaporization first slows down for the highest precursor concentration and ceases after around 9.6 ms ($t/d_0^2 = 0.5$ μs μm^{-2}) of burning, indicated by a constant droplet diameter of 62 μm ($d_p^2/d_0^2 = 0.2$). The linear decrease of the averaged normalized squared droplet diameter with time proceeds longest for pure ethanol for which it slows down and ceases after ~5.1 ms ($t/d_0^2 = 0.5$ μs/μm^2) giving $d_p = 32$ μm ($d_p^2/d_0^2 = 0.1$). The resulting constant droplet size is smallest for pure ethanol and increases with increasing Zn-nitrate concentration to $d_p = 45$, 51, and 62 μm for 0.1, 0.25 and 0.5 mol/L, respectively. The initially similar decrease in droplet size can be attributed to the preferential vaporization of the highly volatile ethanol that combusts in the surrounding flame.[10] Some of the water vapor generated in the reaction diffuses back, condenses onto the droplet due to the low surface temperature close to the ethanol boiling point[22] and mixes with the ethanol. Ethanol consumption and water enrichment in the droplet finally lead to flame extinction and constant droplet diameters. The faster onset of flame extinction and larger diameters of the remaining droplets with increasing Zn-nitrate concentration can be attributed to the initially lower ethanol and higher water contents (water of crystallization released by dissolution of Zn-nitrate nonahydrate). Assuming constant liquid density of water at 20°C and that no water is vaporized during combustion, the expected droplet diameters upon extinction for the 0.1/0.25/0.5 mol/L Zn-nitrate solutions are 27.4, 37.5, and 52.6 μm, respectively. This is in reasonable agreement with the measured droplet sizes of 45, 51, and 62 μm. The larger measured values are attributed to the recondensing water vapor and residual ethanol inside the droplets.

Figure 4 shows the droplet diameter evolution from the analysis of image sequences for (a) Zn-naphthenate/ethanol and (b) Zn-naphthenate/xylene with 0.5 (green line), 0.25 (red), and 0.1 mol/L (blue) Zn concentration as well as the pure solvents (black). For ethanol-based precursors (Figure 4a), a similar initial linear decrease of d_p^2/d_0^2 vs. time is observed as for the nitrate solutions. This confirms that the highly volatile solvent preferentially vaporizes during the early combustion stage. However, the decrease in droplet size ceases rapidly after 1.4 ms ($t/d_0^2 = 0.1$ μs/μm^2) for 0.5 mol/L Zn-naphthenate/ethanol and even seems to increase again before the explosion takes place. The lower the initial molar concentration of the Zn-naphthenate, the longer the onset of explosion is delayed.

A similar behavior is observed for xylene as solvent (Figure 4b). Initially, the decrease in droplet size coincides with that for pure xylene (black line), indicating preferential xylene vaporization, followed by a cease of the droplet size that has not been observed with ethanol prior to explosion. The deviation from pure xylene vaporization occurs very early at 0.2, 1.0, and 2.5 ms for 0.5, 0.25, and 0.1 mol/L Zn-naphthenate concentration, respectively. Although, droplet explosions itself take place slightly earlier for the xylene than for ethanol

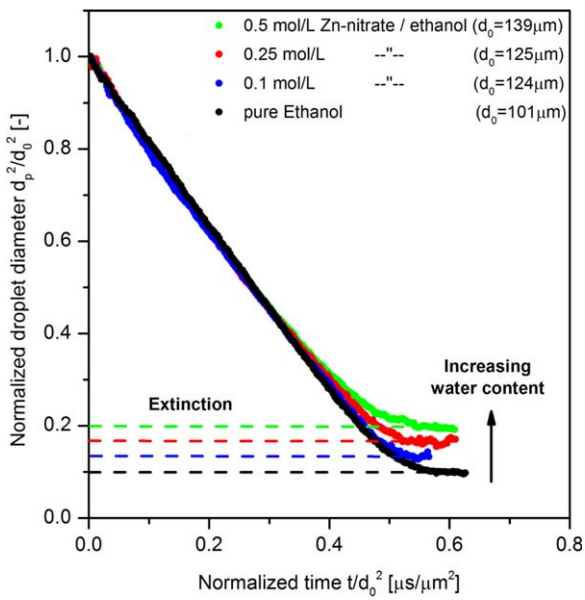

Figure 3. Evolution of the averaged normalized squared droplet diameter for pure ethanol (black, bottom), 0.1 (blue), 0.25 (red), and 0.5 mol/L (green, top) zinc nitrate hexahydrate/ethanol solutions.

[Color figure can be viewed in the online issue, which is available at wileyonlinelibrary.com.]

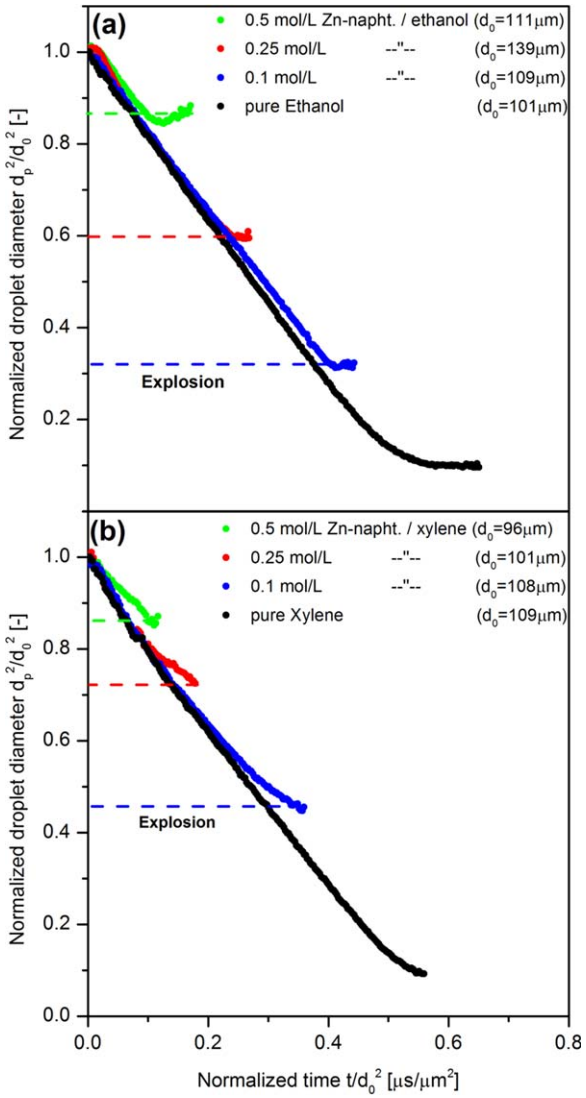

Figure 4. Evolution of the averaged normalized squared droplet diameter for (a) pure ethanol (black, bottom), 0.1 (blue), 0.25 (red), and 0.5 mol/L (green, top) zinc naphthenate/ethanol solutions and (b) pure xylene (black, bottom), 0.1 (blue), 0.25 (red), and 0.5 mol/L (green, top) zinc naphthenate/xylene solutions.

[Color figure can be viewed in the online issue, which is available at wileyonlinelibrary.com.]

solutions, the times until onset of microexplosions are similar. As already shown by Rosebrock et al.[10] for 2-ethylhexanoate metal precursors, these microexplosions are highly reproducible, suggesting similar mechanisms inside the droplets leading to disruptive burning: (1) The less-volatile Zn-naphthenate accumulates at the droplet surface as the solvent preferentially vaporizes. (2) It acts as a diffusion barrier for the solvent, slowing down solvent vaporization and increasing the surface temperature due to the higher naphtenate boiling point (~100 to ~350°C, see Figure 5). (3) The temperature increase will lead both to thermal decomposition of the Zn-naphthenate and superheating of the solvent, causing nucleation of vapor bubbles inside the droplet. (4) Increasing internal pressure and/or expansion of vapor bubbles disrupt the droplet by overcoming the cohesive surface tension forces. In particular, steps (3) and (4) can be readily observed for the Zn-naphthenate/ethanol solutions (Figure 4a), indicated by constant or even increasing droplet size prior to microexplosion. The difference in slope between the vaporization of Zn-naphthenate/xylene and pure xylene (Figure 4b) suggests step (2), i.e., the Zn-naphthenate at the droplet surface accumulates and slows down xylene vaporization. The Zn-naphthenate precursor contains white spirits, which may affect vaporization. However, their boiling points are in the same range as that of xylene and thus should not contribute to the deviations, which occur only for large boiling point differences.[23] The good agreement between the onset of micro explosions for the Zn-naphthenate/ethanol and xylene solutions suggests that the solvent plays a minor role for microexplosions, whereas the nature of the metal precursor seems to be dominating.

The different vaporization behavior of the precursor solutions is illustrated in Figure 5 showing the TGA weight loss (solid lines, left axis) and DSC signal (dotted lines, right axis) of the 0.5 mol/L solutions containing Zn-naphthenate/xylene (green), Zn-naphthenate/ethanol (red), and Zn-nitrate/ethanol (blue) when heated up to 600°C in air at 7.5°C/min. Note that solvent evaporation from the crucible occurs prior to data recording, leading to initial relative masses of 82, 85, and 96 wt %. The Zn-nitrate/ethanol solution (blue) shows a weight loss of ~85 wt % during balance stabilization at 30°C, which is accompanied by heat uptake (positive signal in DSC). This indicates evaporation of ethanol that constitutes 83 wt % of the starting solution, while Zn-nitrate is likely to recrystallize. The subsequent minor weight loss and exothermic step of ~5 wt % around 75°C, can be attributed to the release of water or residual ethanol and starting decomposition/oxidation of Zn-nitrate to ZnO and NOx,[24,25] respectively. These processes seem to continue until at ~325°C, a constant residual weight of 4.3 wt % is obtained. This agrees well with calculated 4.5 wt % ZnO, based on the composition of the starting solution.

TGA results are in line with the single-droplet study (Figure 3), showing solvent evaporation and subsequent formation of zinc nitrate or zinc oxide residues.

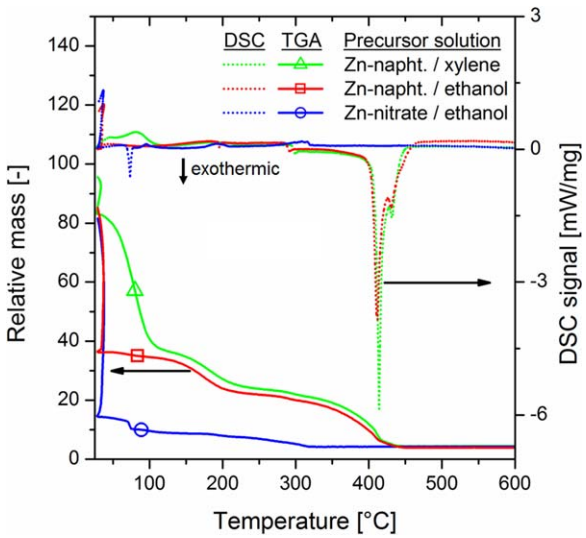

Figure 5. Normalized TGA weight loss (solid line, left axis) and DSC signal (dotted line, right axis) for zinc nitrate hexahydrate/ethanol (blue), zinc naphthenate/ethanol (red), and zinc naphthenate/xylene (green) solutions.

[Color figure can be viewed in the online issue, which is available at wileyonlinelibrary.com.]

A similar albeit smaller initial weight loss and endothermic signal are observed for the zinc naphthenate/ethanol solution (red lines). It proceeds till 36 wt % of the initial mass is reached and agrees well with the starting ethanol content of 39 wt %. The following weight loss of ~15 wt % between 100 and 250°C may be attributed to vaporization of mineral spirits (13.5 wt % in starting solution). The subsequent mass loss of ~11 wt %, which is accompanied by a large exothermic DSC signal around 400°C is ascribed to naphthenate decomposition/oxidation[26] leading to ZnO. Again, the final residual weight of 4.0 wt % compares well with expected 4.5 wt % ZnO. Zn-naphthenate/xylene behaves similar to the ethanol solution except for the shift of the initial weight loss of ~62 wt % to higher temperatures (63 wt % of xylene in starting solution) and a less-pronounced endothermic signal. The former is attributed to the higher boiling point of xylene compared to ethanol (~139 vs. 78°C)[27] and the latter to the lower specific heat of vaporization (336 vs. 837 kJ/kg).[27]

The maximum superheat temperatures to which liquids may be heated at 1 atm before vapor bubble nucleation must occur are 189.5°C and 235°C[28] for ethanol and xylene, respectively. These can be readily exceeded for Zn-naphthenate, whereas the decomposition of Zn-nitrate is almost finished before reaching these limits (Figure 5). Such superheated liquids boil explosively,[28] explaining the occurrence of microexplosions in naphthenate-based solutions (Figures 2b, c) and their absence in nitrate-based (Figure 2a) solutions. This is in agreement with former results,[10] showing that high precursor-decomposition temperatures and multiple decomposition steps promote microexplosions. The residues in TGA that compare well with the calculated amount of zinc oxide based on the starting Zn concentrations indicate that also the naphthenate precursor does not vaporize from the droplets, as may be expected. Instead, the microexplosions seem to be essential to distribute the precursor or its decomposition products in the gas phase.

Figure 6 shows TEM images of ZnO nanoparticles sampled from single burning droplet (a–f) and lab-scale FSP reactor (g–l) experiments, employing 0.5 mol/L precursor solutions of Zn-naphthenate/xylene (left), Zn-naphthenate/ethanol (middle), and Zn-nitrate/ethanol (right). Single droplet combustion yields fine agglomerated ZnO nanoparticles for Zn-naphthenate solutions (Figures 6a, d and b, e). The particles are slightly elongated or sphere-like with sizes mostly around 10–20 nm, as has been observed previously in flame spray synthesis of ZnO nanopowders[29,30] and compares well with the FSP-made particles of the same precursor solution (Figures 6g, j and h, k). This rather surprising agreement between products of single droplet and spray combustion may be partly due to similar time scales for particle growth. Droplet combustion takes place in 1 to 10 ms (Figure 4b) which is also the time for primary particle growth in FSP reactors, as shown for zirconia by burning a Zr-2-ethylhexanoate/xylene precursor solution[20] that is chemically similar to the Zn-naphthenate/xylene precursor here.

Combustion of Zn-nitrate/ethanol droplets shows large patches without any appreciable ZnO nanoparticles (Figures 6c, f). The structure of these deposits with sphere-like center and scattered fragments suggests that the single droplets observed in the image sequence (Figure 2a) survive till they impact on the TEM grid and possibly dry thereafter. The size of the deposits of some tens of micrometers is of similar magnitude as the constant droplet diameter upon flame extinction (Figure 3). It seems that the impacting droplets had a shell-like structure, indicating nitrate precursor precipitation upon solvent vaporization[12,13] as in conventional spray pyrolysis[31] and in agreement with large hollow or solid spherical particles typically observed in the FSP product powder of nitrate precursors.[15,16,32] The corresponding FSP-made ZnO nanopowders here (Figures 6i, l) however consist of homogeneous spherical or slightly elongated nanoparticles resembling those of the two other precursor solutions (Figures 6g, j and h, k). Large and partially hollow particles stemming from droplet-to-particle conversion are not detected and, to the best of our knowledge, have never been reported for FSP-made zinc oxide.

In contrast to the single droplet experiments, the large droplets/particles in the FSP flame are likely to undergo further vaporization due to the high temperature environment. Note that ZnO starts to melt and decompose into zinc vapor and oxygen at around 2000°C[33] at ambient pressure. In ethanol/oxygen spray flames temperatures of 2100–2700°C are readily obtained.[7,34] Oxygen-deficient flame zones revealed by computational fluid dynamics in such flames[34] may further facilitate ZnO decomposition. Micron-sized ZnO particles originating from the observed precursor droplets (Figure 6c and f) are thus likely to fully decompose into zinc and oxygen, providing Zn vapor for renucleation of ZnO nanoparticles in colder flame regions.[35]

This proposed formation mechanism for ZnO nanoparticles is traced by thermophoretically sampling at 5, 15, and 25 cm HAB on the centerline of 0.5 mol/L Zn-nitrate/ethanol (Figures 7a–c) and Zn-naphthenate/xylene (Figures 7d–f) FSP flames. The study was performed with the pilot-scale FSP reactor as the physicochemical mechanisms proceed over longer distances than in the smaller lab-scale reactor, spatially separating the different precursor release and particle formation steps.

Figure 7a shows a sample taken early in the flame at 5 cm HAB. A single, relatively large particle (~100 nm diameter) is observed along with some small (~10 nm) nanoparticles. The background seems to consist of patches that are difficult to discern but at higher resolution, appear as continuous polycrystalline coating (confirmed by selected area electron diffraction, data not shown) with 10–20 nm large crystals. In scanning electron microscopy (data not shown) these patches fully cover the grid similar to sputter-deposition. This indicates the condensation of Zn vapor present in the flame at this HAB onto the cold TEM grid. Thus, large particles made by droplet-to-particle conversion (Figures 6c, f) are indeed present early in the spray flame, but seem to evaporate by ZnO decomposition in the high temperature reducing environment. At 15 cm HAB (Figure 7b), neither the large particles nor the sputter-like coatings are observed, in line with the homogeneous product powder of the lab-scale reactor (Figures 6i, l). Spherical and rod-like nanoparticles that partially form agglomerates are uniformly distributed across the grid. Apparently, the Zn vapor present upstream the flame has condensed in colder flame regions at the larger HAB forming ZnO nanoparticles. At 25 cm HAB (Figure 7c), ZnO particles seem to be larger and are more agglomerated.

Thermophoretic sampling in the hotter Zn-naphthenate/xylene pilot-scale flame at 5 (Figure 7d), 15 (Figure 7e), and 25 cm HAB (Figure 7f) does not show any large particles made by droplet-to-particle conversion. This is in agreement with the droplet disruption by microexplosions (Figures 2b, c) and homogeneous product powders from single-droplet combustion (Figures 6a, d and b, e). Note that the sputter-like coatings are observed at 5 and 15 cm HAB (Figures 7d, e) while

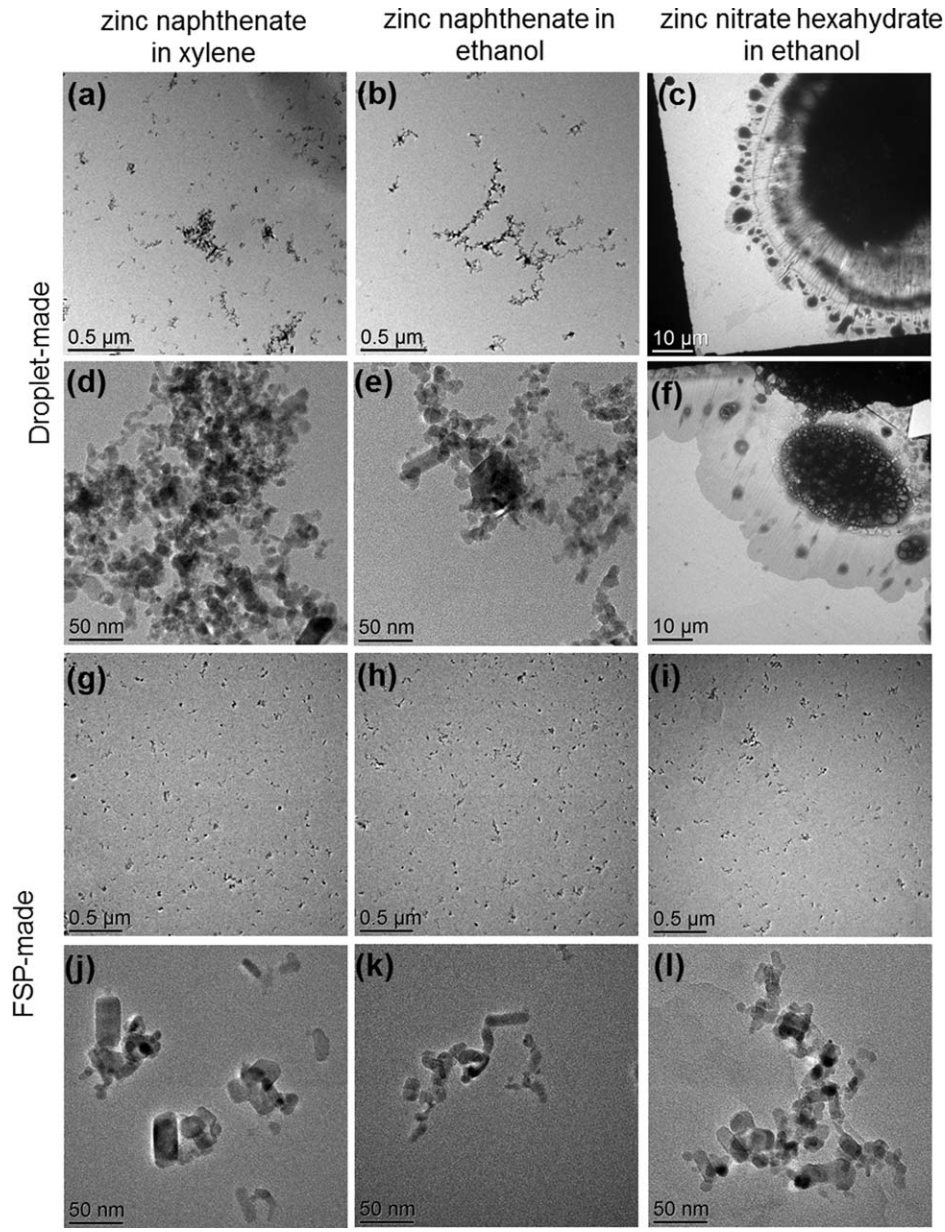

Figure 6. TEM images of ZnO nanoparticle samples made from single droplets (a–f) and lab-scale FSP at 25 cm HAB (g–l) of 0.5 mol/L Zn-naphthenate/xylene (left), 0.5 mol/L Zn-naphthenate/ethanol (middle), and 0.5 mol/L Zn-nitrate/ethanol (right).

nanoparticles have only formed at 25 cm HAB (Figure 7f). This is attributed to the higher temperatures of the xylene-based flame compared to the ethanol one. Gröhn et al.[20] reported for such flames ~2200°C at 15 cm HAB, which is well above the dissociation temperature of ZnO. At 25 cm HAB, they measured temperatures around 1300°C, lower than the thermal dissociation temperature of ZnO (2000°C[33]) and in line with the presence of ZnO nanoparticles (Figure 7f).

In summary, neither zinc nitrate nor zinc naphthenate seem to directly vaporize from the droplets but form a shell. The high decomposition temperature of the naphthenate allows solvent superheating that leads to microexplosions and homogeneous product nanopowders, independent of the solvent. Zinc nitrate/ethanol droplets extinguish and the precursor decomposes before superheating/microexplosions can take place. However, the resulting large ZnO particles formed by droplet-to-particle conversion decompose in the FSP flame that is hotter than the decomposition temperature of ZnO. Thus, homogeneous nanopowders are obtained from Zn vapor also for Zn-nitrate/ethanol precursor solutions.

Iron and aluminum oxides

Al_2O_3 and Fe_2O_3 possess higher thermal stability (volatilization/boiling point temperature of Al_2O_3 is 3000°C,[27] whereas Fe_2O_3 forms Fe_3O_4 at 1460°C,[36] which has an volatilization temperature of 2623°C[37]) compared to ZnO (starting at ~2000°C[33]). Thus, inhomogeneous product nanopowders are expected for nitrate-based precursor solutions.[13]

Figure 8 shows image sequences of single burning droplets composed of 0.5 mol/L (a) Fe-nitrate/ethanol (~5.5 ms) and (b) Al-nitrate/ethanol (~4 ms). In contrast to Zn-nitrate/ethanol, small microexplosions can be observed for Fe-nitrate

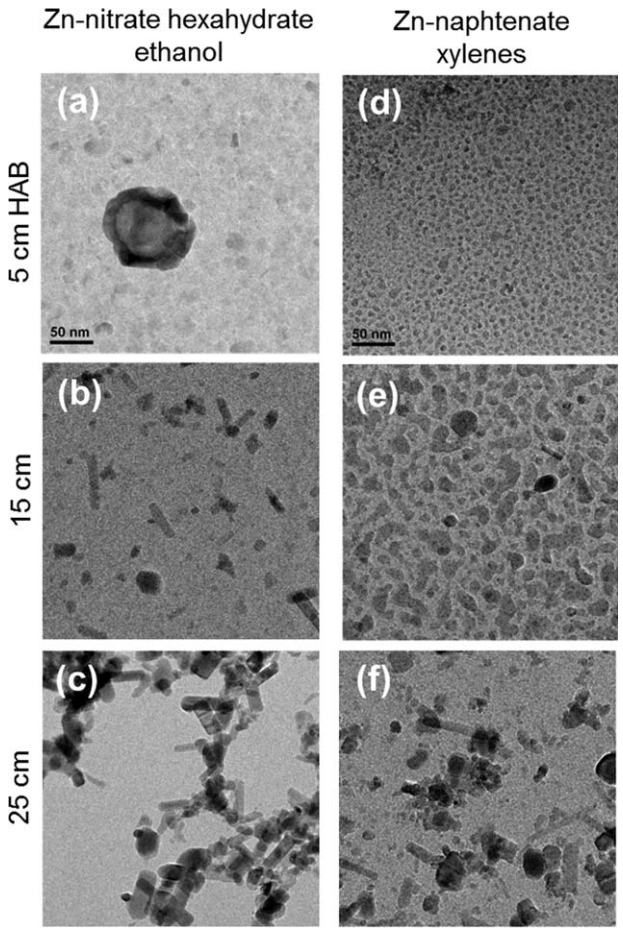

Figure 7. TEM images of samples taken thermophoretically at 5 (top), 15 (middle), and 25 cm (bottom) HAB *in situ* a pilot-scale flame producing ZnO from 0.5 mol/L Zn-nitrate/ethanol (a–c, left) or Zn-naphthenate/xylene (d–f, right).

while Al-nitrate exhibits disruptions that are almost comparable to the Zn-naphthenate solutions (Figures 2b, c). However, the fragments of microexplosions for both nitrate-based solutions are prone to flame extinction similar to Zn-nitrate/ethanol.

Quantitative results are presented in Figure 9, showing the averaged normalized squared droplet diameter for pure ethanol (black) and 0.5 mol/L solutions of Al-nitrate (green) and Fe-nitrate (red) along with the Zn-nitrate data (blue; see Figure 3) for comparison. Initially, all droplets shrink similarly in diameter up to $t/d_0^2 = 0.1$ μs μm^{-2}, confirming the preferential vaporization of ethanol. After approximately 20, 40, and 60% reduction of the initial squared droplet diameter, vaporization decreases for Fe-nitrate (red), Al-nitrate (green), and Zn-nitrate solutions (blue), respectively, indicated by a deviation from the pure ethanol curve.

The corresponding droplet diameters at extinction are 56 (Fe-nitrate), 58 (Al-nitrate), and 62 μm (Zn-nitrate). Note that the increase and data scattering for Al-nitrate are due to the deformation of the droplet after the microexplosions. Flame extinction occurs faster for initially higher water and lower ethanol contents in the droplets, as seen already for increasing Zn-nitrate concentration (Figure 3). Neglecting the influence of the microexplosions, 0.5 mol/L Zn-nitrate, Fe-nitrate and Al-nitrate solutions contain approximately 36, 40, and 43% water per gram nitrate, respectively, in line with the extinction order.

Figure 10 shows the weight loss (solid lines, left axis) and DSC signal (dotted lines, right axis) of precursor solutions containing 0.5 mol/L Fe-nitrate/ethanol (green) and Al-nitrate/ethanol (red) when heated up to 600°C in air at 7.5°C/min. Again, the high volatility of ethanol leads to smaller relative masses of 83 and 84 wt % at the start of data recording. The Fe-nitrate/ethanol solution shows an initial weight loss of approx. 80 wt % up to 50°C, which is accompanied by an endothermic (positive) signal in DSC. This weight loss is in excellent agreement with the starting ethanol content of 78 wt %, confirming that ethanol vaporizes preferentially. As with Zn-nitrate, Fe-nitrate is likely to precipitate as the solvent evaporates. The subsequent mass loss of about 10 wt % accompanied by an exothermic peak suggests nitrate decomposition and formation of crystalline iron oxide. The residual mass of 4.3 wt % is in good agreement with the expected 4.4 wt % of Fe_2O_3.

The Al-nitrate/ethanol solution has lost approximately 72% of weight (starting ethanol content: 84 wt %) before a plateau of quasi-constant mass accompanied by a slightly endothermic signal is reached until ~80°C. The following mass loss of 17 wt % between 80 and 100°C is endothermic again. The residual mass of 3.3 wt % is in reasonable agreement with expected 2.8 wt % of Al_2O_3. The plateau is attributed to the melting of the Al-nitrate precipitate formed during solvent evaporation along with formation of intermediate oxynitrates,[38] while hardly any decomposition and release of water or residual ethanol takes place. These seem to be removed in the subsequent step up to 100°C.

The absence of an exothermic peak contrary to Zn- and Fe-nitrate/ethanol solutions suggests the formation of an amorphous instead of a crystalline structure. Similar observations have been made in the TGA of aluminum nitrate powder exposed to air and nitrogen,[38,39] which pointed at the endothermic formation of intermediates such as aluminum oxynitrate and hydroxyide rather than crystalline Al_2O_3. The initial mass loss till the attainment of the plateau indicates that not all ethanol vaporized. As the boiling point of ethanol lies within the region of the plateau, the oxynitrate intermediates may act as seeds for ethanol vapor bubble nucleation in the droplets, readily leading to the observed microexplosions. However, due to the large amount of water still present in the droplets (see water release between 80 and 100°C in TGA), flame extinction occurs after the microexplosion, probably leading to large inhomogeneous nanoparticles as frequently observed for nitrate-based metal precursors.[13]

Figure 11, showing TEM images of Al_2O_3 (left) and iron oxide (right) particles made by single-droplet combustion (Figures 11a–d) and lab-scale FSP (Figures 11e–h) from the 0.5 mol/L nitrate/ethanol solutions, confirms the proposed

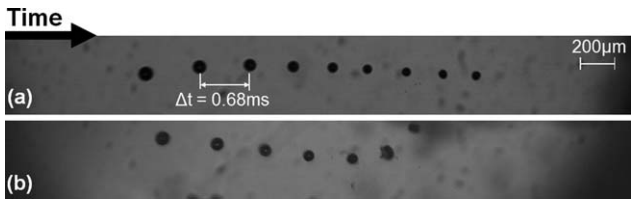

Figure 8. Image sequences of single burning droplets composed of 0.5 mol/L (a) Fe-nitrate/ethanol and (b) Al-nitrate/ethanol.

The time interval between two successive droplet images is 0.68 ms. The initial droplet diameters are (a) 90 μm and (b) 95 μm, respectively.

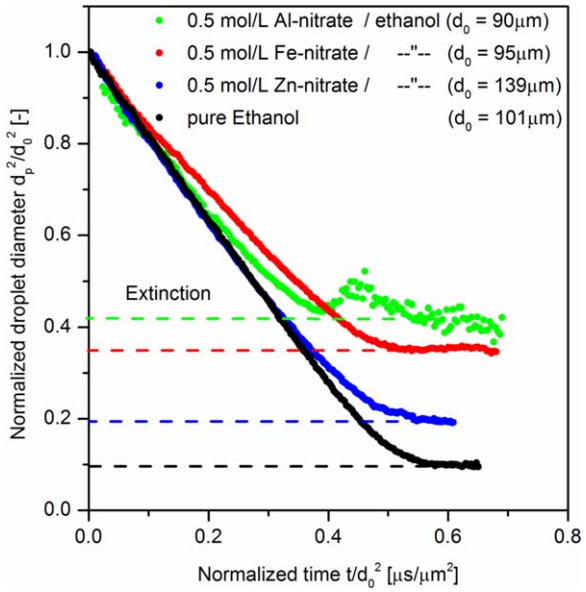

Figure 9. Evolution of the averaged normalized squared droplet diameter for pure ethanol (black, bottom) as well as solutions in ethanol of 0.5 mol/L Zn-nitrate (blue), Fe-nitrate (red), and Al-nitrate (green, top).

[Color figure can be viewed in the online issue, which is available at wileyonlinelibrary.com.]

formation mechanisms. Single-droplet combustion leads to large spherical particles without any appreciable fine nanoparticles (Figures 11a–d) in line with the observations for ZnO (Figures 6c, f). The sphere-like structures with size similar to the extinction diameters (Figure 9) and the absence of scattered fragments suggest complete solidification upon impact onto the TEM grid, contrary to ZnO (Figures 6c, f). The reason might be volume precipitation effects within the droplets for the Al- and Fe-nitrate/ethanol solutions. Volume precipitation is favored for a uniform concentration throughout the interior of the droplet,

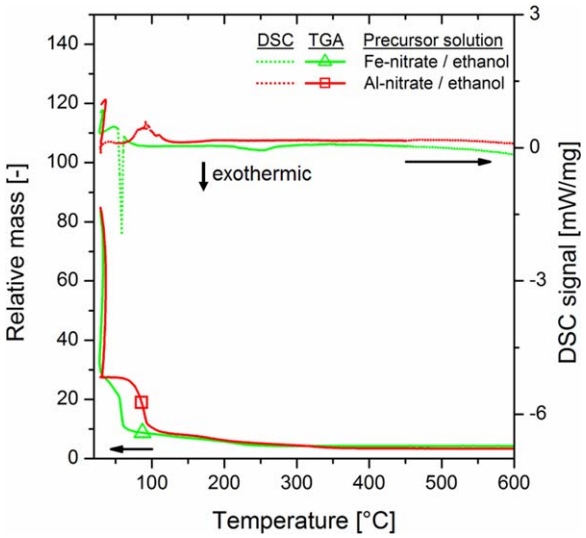

Figure 10. Normalized TGA (solid line, left axis) and DSC (dotted line, right axis) measurements for iron (green) and aluminum (red) nitrate nonahydrate in ethanol.

[Color figure can be viewed in the online issue, which is available at wileyonlinelibrary.com.]

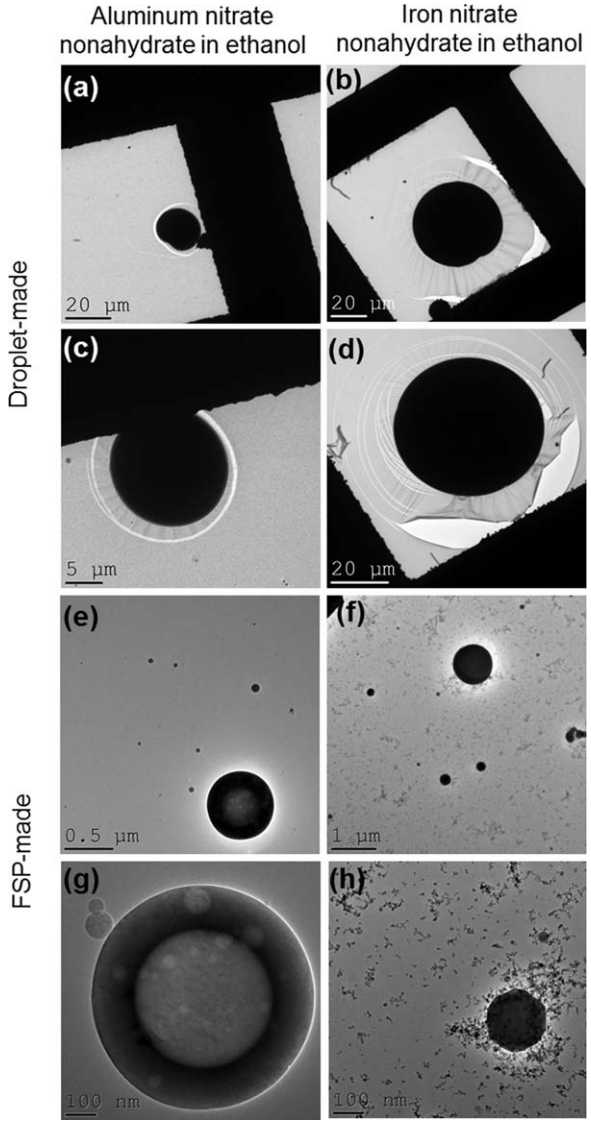

Figure 11. TEM images of Al_2O_3 (left) and iron oxide (right) samples made from single droplets (a–d) and lab-scale FSP (e–f) of 0.5 mol/L Al-nitrate/ethanol and Fe-nitrate/ethanol.

which can be attained by low vaporization rates and internal mixing effects.[31] The microexplosions occurring for Al- and Fe-nitrate/ethanol solutions may lead to internal mixing, while the following extinction reduces the vaporization rate. This is contrary to Zn-nitrate/ethanol, where microexplosions are absent.

Lab-scale FSP experiments for the Al-nitrate/ethanol solution (Figures 11e, f, left) yield large partially hollow submicron-sized particles along with a few nanoparticles. The Fe-nitrate/ethanol solution (Figures 11f, h, right) gives similar products but a larger nanoparticle fraction. These results along with the findings for ZnO indicate that large particles made by droplet-to-particle conversion will end up in the FSP product powder only if the thermal dissociation temperature of the product material is higher than the FSP flame temperature.

Metal carboxylates

Although iron and in particular aluminum nitrate-based precursors exhibit initial microexplosions, inhomogeneous nanopowders are observed attributed to flame extinction. If fragments

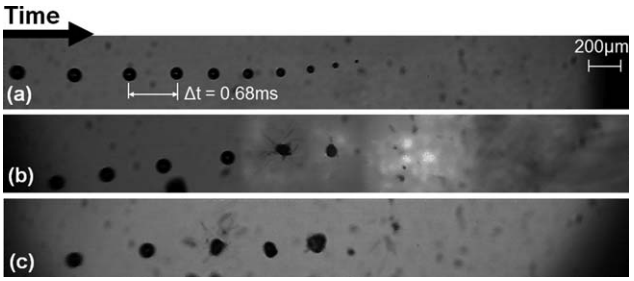

Figure 12. Image sequences of single burning droplets composed of (a) ethanol/xylene/DEGBE/EHA (1:1:1:1 volume ratio), (b) 0.5 mol/L Fe-nitrate, and (c) Al-nitrate in ethanol/xylene/DEGBE/EHA (1:1:1:1 volume ratio).

The time interval between two successive droplet images is 0.68 ms. The initial droplet diameters are (a) 94 μm, (b) 90 μm, and (c) 94 μm, respectively.

continued to burn, ongoing cascade-like microexplosions and progressing vaporization should result in homogeneous nanopowders. Strobel and Pratsinis[13] proposed a solvent mixture of ethanol/xylene/diethyleneglycol monobutyl ether (DEGBE)/2-ethylhexanoic acid (EHA) in equal volumes to obtain homogeneous nanoparticles for metal nitrates. This mixture is assumed to form metal carboxylate complexes comparable to 2-ethylhexanoate precursors that should facilitate cascade-like microexplosions and gas-to-particle conversion.

Figure 12 shows image sequences of single burning droplets composed of the proposed solvent mixture, where (a) is precursor-free (~6.1 ms), (b) with 0.5 mol/L Fe-nitrate (~4 ms), and (c) with 0.5 mol/L Al-nitrate (~3.4 ms). It can be seen from Figure 12a that the pure mixture burns continuously without any microexplosions or flame extinction. In contrast, the Fe- and Al-nitrate solutions (Figures 12b, c) show disruptive burning, where the droplet fragments continue to burn until they are completely consumed. The observed microexplosions are similar to those observed for Zn-naphtenate (Figures 2b, c) and comparable to previous results,[10] indicating that the metal 2-ethylhexanoate complex is formed, indeed.

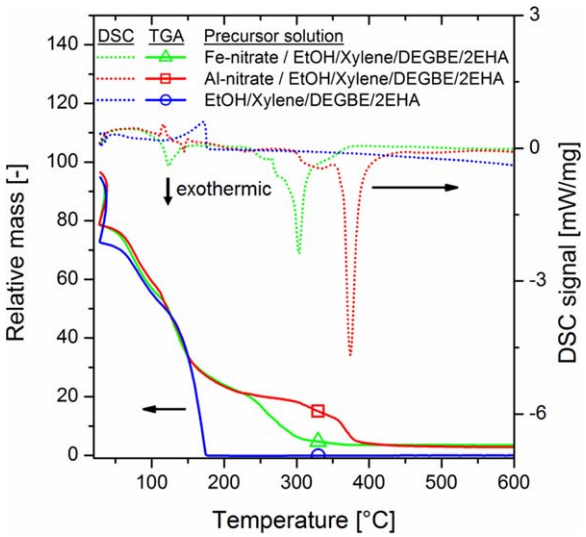

Figure 13. Normalized TGA mass loss (solid line, left axis) and DSC signal (dotted line, right axis) for iron (green) and aluminum (red) nitrate nonahydrate in ethanol/xylene/DEGBE/EHA (1:1:1:1 volume ratio) and the corresponding pure mixture (blue).

[Color figure can be viewed in the online issue, which is available at wileyonlinelibrary.com.]

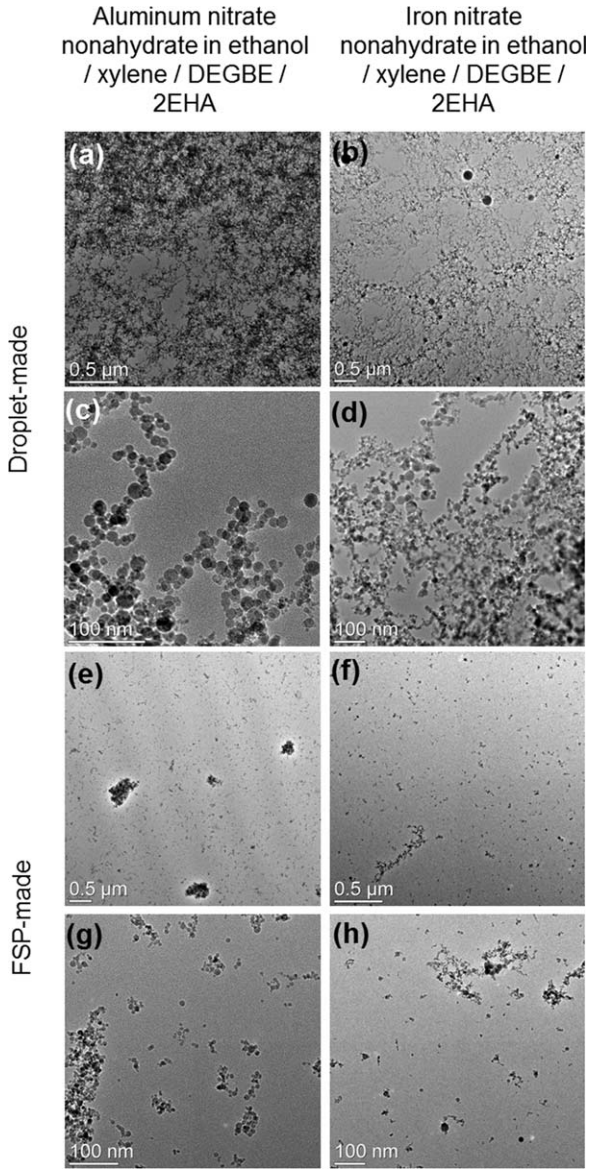

Figure 14. TEM images of Al_2O_3 (left) and iron oxide (right) nanoparticles sampled from single droplet combustion (a–d) and lab-scale FSP (e–h) of 0.5 mol/L Al-nitrate and Fe-nitrate in ethanol/xylene/DEGBE/EHA.

Figure 13 shows the TGA of the Fe- (green) and Al-nitrate/ethanol/xylene/DEGBE/EHA solutions (red) along with the pure solvent mixture (blue). Note again that some evaporation takes place prior to data recording, leading to initial rel. masses of ~95 wt %. In accordance with Figure 12a, the pure solvent mixture vaporizes completely and without residue up to ~180°C. The DSC signal (dotted blue line) shows only endothermic signals attributed to the different heats of vaporization.

The mass losses of Fe- (green) and Al-nitrate solutions (red) first resemble that of the pure solvent mixture, but start to deviate after approx. 70 wt % have been vaporized at ~150°C. This is similar to the initial mass fraction of ethanol, xylene, and DEGBE of 74.3 wt %. Subsequently, two mass loss steps

over a wide temperature range are observed, a slower and slightly endothermic one followed by a fast and highly exothermic one. These decomposition steps can be attributed to carboxylate complexes, formed by the 2-ethylhexanoic acid and the metal ions in the solutions, as suggested by Strobel and Pratsinis.[13] Metal carboxylates typically decompose in a two- or three-step process to the metal oxides,[40] as observed also for Zn-naphthenate (Figure 5). The residual masses of 3.5 and 2.9 wt % for the Fe- and Al-nitrate solutions agree well with the expected 4.0 and 2.6 wt % of Fe_2O_3 and Al_2O_3, respectively.

The TGA data suggest that the observed cascade-like microexplosions (Figures 12b, c) are associated with the formation of high boiling point carboxylate complexes in the droplets and superheating of solvent residues rather than due to the multicomponent solvent mixture. The nanopowders from these metal nitrate solvent mixtures[13] are thus expected to be homogeneous.

Figure 14 shows the comparison of droplet- and FSP-made nanoparticles of 0.5 mol/L Fe-nitrate (right) and Al-nitrate (left) dissolved in ethanol/xylene/DEGBE/EHA (1:1:1:1 volume ratio). Homogeneous fine agglomerated iron and aluminum oxide nanoparticles are produced from the single burning droplets (Figures 14 a–d). Similar results are observed for the FSP-made nanopowders (Figures 14 e–h), confirming that the proposed solvent mixture[13] facilitates gas-to-particle conversion for homogeneous product nanopowders through carboxylate formation and cascade-like microexplosions.

Conclusions

Single-droplet combustion experiments along with TGA showed that homogeneous nanopowders are formed in flame spray pyrolysis when droplets undergo cascade-like microexplosions, independent of precursor volatility or nature of the solvents. Such microexplosions take place for metal precursors that decompose in multiple steps over a wide temperature range exceeding the boiling points of the solvents, therefore triggering disruptions by vapor bubble nucleation inside the droplets. It was shown that combustion of the explosion fragments needs to proceed to give homogeneous nanopowders. Examples of such precursors are 2-ethylhexanoates or naphthenates, which may also be formed *in situ* the precursor solution by combining for instance a metal nitrate and 2-ethylhexanoic acid.

Inhomogeneous nanopowders are obtained by droplet-to-particle conversion from precursor solutions that are prone to flame extinction, even if initial microexplosions take place. Extinction during droplet combustion can occur by water condensation and accumulation in the droplet, e.g., for solvents miscible with water and of lower boiling point than water such as metal nitrate/ethanol solutions. In case droplet-to-particle conversion takes place, homogeneous nanopowders may still be obtained if the decomposition or volatilization temperature of the product material is lower than the flame temperature. This was observed here for ZnO that initially formed large particles from zinc-nitrate/ethanol droplets which decomposed again in the high temperature flame environment.

Intelligent design of precursor-solvent mixtures that fulfill the requirements for cascade-like droplet microexplosions will allow the production of homogeneous nanopowders even from low-cost inorganic precursors, reducing production costs and making the FSP technology even more attractive for industrial manufacture of fine particles.

Acknowledgments

The authors would like to thank the Deutsche Forschungsgemeinschaft (DFG) for funding this project under grants of MA 3333/4-1. The authors also thank Andrej Gorzawski from the Department of Manufacturing Technologies (Foundation Institute of Materials Science (IWT), University of Bremen) for providing the high-speed camera, Thorsten Mehrtens from the Institute of Solid State Physics (University of Bremen) and Frank Krumeich (ETH Zurich) for the TEM analyses. Karsten Wegner kindly acknowledges funding from the Swiss National Science Foundation and ETH Zurich, R'Equip grant 206021-113114/1.

References

1. Mezey EJ. *Pigments and Reinforcing Agents*. New York: Wiley, 1966.
2. Buxbaum G. *Industrial Inorganic Pigments*. Weinheim: Wiley-VCH, 1998.
3. Kruis FE, Fissan H, Peled A. Synthesis of nanoparticles in the gas phase for electronic, optical and magnetic applications—a review. *J. Aerosol. Sci*. 1998;29(5–6):511–535.
4. Strobel R, Pratsinis SE. Flame aerosol synthesis of smart nanostructured materials. *J Mater Chem*. 2007;17(45):4743–4756.
5. Cushing BL, Kolesnichenko VL, O'Connor CJ. Recent advances in the liquid-phase syntheses of inorganic nanoparticles. *Chem Rev*. 2004;104(9):3893–3946.
6. Kammler HK, Mädler L, Pratsinis SE. Flame synthesis of nanoparticles. *Chem Eng Technol*. 2001;24(6):583–596.
7. Mädler L, Kammler HK, Müller R, Pratsinis SE. Controlled synthesis of nanostructured particles by flame spray pyrolysis. *J Aerosol Sci*. 2002;33(2):369–389.
8. Teoh WY, Amal R, Mädler L. Flame spray pyrolysis: an enabling technology for nanoparticles design and fabrication. *Nanoscale*. 2010;2(8):1324–1347.
9. Wegner K, Schimmoeller B, Thiebaut B, Fernandez C, Rao TN. Pilot plants for industrial nanoparticleproduction by flame spray pyrolysis. *Kona Powder Part J*. 2011;(29):251–265.
10. Rosebrock CD, Riefler N, Wriedt T, Mädler L, Tse SD. Disruptive burning of precursor/solvent droplets in flame-spray synthesis of nanoparticles. *AIChE J*. 2013;59(12):4553–4566.
11. Noriler D, Rosebrock CD, Mädler L, Meier HF, Fritsching U. Influence of atomization and spray parameters on the flame spray process for nanoparticle production. *Atomization Sprays*. 2014;24(6):495–524.
12. Jossen R, Pratsinis SE, Stark WJ, Mädler L. Criteria for flame-spray synthesis of hollow, shell-like, or inhomogeneous oxides. *J Am Ceram Soc*. 2005;88(6):1388–1393.
13. Strobel R, Pratsinis SE. Effect of solvent composition on oxide morphology during flame spray pyrolysis of metal nitrates. *Phys Chem Chem Phys*. 2011;13(20):9246–9252.
14. L. Mädler, Stark WJ, Pratsinis SE. Flame-made ceria nanoparticles. *J Mater Res*. 2002;17:1356–1362.
15. Jossen R, Mueller R, Pratsinis SE, Watson M, Akhtar MK. Morphology and composition of spray-flame-made yttria-stabilized zirconia nanoparticles. *Nanotechnology*. 2005;16(7):609–617.
16. Mädler L, Pratsinis SE. Bismuth oxide nanoparticles by flame spray pyrolysis. *J Am Ceram Soc*. 2002;85(7):1713–1718.
17. Stark WJ, Madler L, Maciejewski M, Pratsinis SE, Baiker A. Flame synthesis of nanocrystalline ceria-zirconia: effect of carrier liquid. *Chem Commun*. 2003(5):588–589.
18. Ulmke H, Mietschke M, Bauckhage K. Piezoelectric single nozzle droplet generator for production of monodisperse droplets of variable diameter. *Chem Eng Technol*. 2001;24(1):69–70.
19. Riefler N, Wriedt T. Generation of monodisperse micron-sized droplets using free adjustable signals. *Part Part Syst Charact*. 2008; 25(2):176–182.
20. Gröhn AJ, Pratsinis SE, Sanchez-Ferrer A, Mezzenga R, Wegner K. Scale-up of nanoparticle synthesis by flame spray pyrolysis: the high-temperature particle residence time. *Ind Eng Chem Res*. 2014; 53(26):10734–10742.
21. Dobbins RA, Megaridis CM. Morphology of flame-generated soot as determined by thermophoretic sampling. *Langmuir*. 1987;3(2):254–259.
22. Lee A, Law CK. An experimental investigation on the vaporization and combustion of methanol and ethanol droplets. *Combust Sci Technol*. 1992;86(1-6):253–265.

23. Wang CH, Liu XQ, Law CK. Combustion and microexplosion of freely falling multicomponent droplets. *Combust Flame*. 1984;56(2): 175–197.
24. Mu J, Perlmutter DD. Thermal-decomposition of metal nitrates and their hydrates. *Thermochim Acta*. 1982;56(3):253–260.
25. Malecka B, Gajerski R, Malecki A, Wierzbicka M, Olszewski P. Mass spectral studies on the mechanism of thermal decomposition of Zn(NO3)(2) nH(2)O. *Thermochim Acta*. 2003;404(1–2):125–132.
26. Ohrbach KH, Matuschek G, Kettrup A, Joachim A. Simultaneous thermal-analysis mass-spectrometry on lubricant systems and additives. *Thermochim Acta*. 1990;166:277–289.
27. Lide DR. Handbook of Chemistry and Physics, 88th Ed., Boca Raton: CRC Press., 2007.
28. Blander M, Katz JL. Bubble nucleation in liquids. *AIChE J*. 1975; 21(5):833–848.
29. Height MJ, Mädler L, Pratsinis SE, Krumeich F. Nanorods of ZnO made by flame spray pyrolysis. *Chem Mater*. 2006;18(2):572–578.
30. Wallace R, Brown AP, Brydson R, Wegner K, Milne SJ. Synthesis of ZnO nanoparticles by flame spray pyrolysis and characterisation protocol. *J Mater Sci*. 2013;48(18):6393–6403.
31. Messing GL, Zhang S-C, Jayanthi GV. Ceramic powder synthesis by spray pyrolysis. *J Am Ceram Soc*. 1993;76(11):2707–2726.
32. Tani T, Watanabe N, Takatori K, Pratsinis SE. Morphology of oxide particles made by the emulsion combustion method. *J Am Ceram Soc*. 2003;86(6):898–904.
33. Klimm D, Schulz D, Ganschow S. Bulk crystal growth of semiconductors: an overview. In: Bhattacharya P, Fornari R, Kamimura H, eds. *Comprehensive Semiconductor Science and Technology*. Vol 3. Amsterdam: Elsevier, 2011:302–338.
34. Gröhn AJ, Pratsinis SE, Wegner K. Fluid-particle dynamics during combustion spray aerosol synthesis of ZrO2. *Chem Eng Technol*. 2012;191(0):491–502.
35. Hembram K, Sivaprakasam D, Rao TN, Wegner K. Large-scale manufacture of ZnO nanorods by flame spray pyrolysis. *J Nanoparticle Res*. 2013;15(2):1–11.
36. Stull DR, Prophet H. JANAF Thermochemical Tables, 2nd. Ed., Washington: National Bureau of Standards, 1971.
37. Cornell RM, Schwertmann U. The Iron Oxides: Structure, Properties, Reactions, Occurences and Uses, Weinheim: Wiley-VCH, 2003.
38. Melnikov P, Nascimento VA, Arkhangelsky IV, Consolo LZZ. Thermal decomposition mechanism of aluminum nitrate octahydrate and characterization of intermediate products by the technique of computerized modeling. *J Therm Anal Calorim*. 2013;111(1):543–548.
39. Pacewska B, Keshr M. Thermal transformations of aluminium nitrate hydrate. *Thermochim Acta*. 2002;385(1–2):73–80.
40. Mishra S, Daniele S, Hubert-Pfalzgraf LG. Metal 2-ethylhexanoates and related compounds as useful precursors in materials science. *Chem Soc Rev*. 2007;36(11):1770–1787.

Manuscript received Aug. 11, 2015